Noise-induced transitions in a double-well oscillator with nonlinear dissipation

Vladimir V. Semenov,[1, *] Alexander B. Neiman,[2, †] Tatyana E. Vadivasova,[1] and Vadim S. Anishchenko[1]

[1]*Department of Physics, Saratov State University,*
Astrakhanskaya str., 83, 410012, Saratov, Russia
[2]*Department of Physics and Astronomy, Ohio University, Athens, Ohio 45701, USA*

(Dated: January 5, 2016)

We develop a model of bistable oscillator with nonlinear dissipation. Using an electronic circuit realization of this system we study its response to noise excitations experimentally. We show that depending on noise intensity the system undergoes multiple qualitative changes in the structure of its steady-state probability density function (PDF). In particular, the PDF exhibits two pitchfork bifurcations vs noise intensity, which we describe using an effective potential and corresponding normal forms of bifurcations. These stochastic effects are explained by the partition of the phase space by the nullclines of the system.

Introduction – Bistable dynamics is typical for many natural systems in physics [1–3], chemistry [4, 5], biology [6–11], ecology [12, 13], geophysics [14–16]. The simplest kind of bistability occurs when a system possesses two stable equilibria in the phase space, separated by a saddle. Adding noise gives rise to random switchings between the deterministically stable states, resulting in a steady state probability density with two local maxima. The Kramers oscillator is a classical example of the stochastic bistable system describing Brownian motion in the double-well potential [2, 4, 17],

$$\dot{y} = v, \quad \dot{v} = -\gamma v - \frac{dU(y)}{dy} + \sqrt{2\gamma D}\, n(t), \quad (1)$$

where γ is the (constant) drag coefficient, $U(y)$ is a double-well potential and $n(t)$ is Gaussian white noise, D is the noise intensity. Two-dimensional equilibrium PDF is:

$$P(y, v) = k \exp\left[-\frac{1}{D}\left(\frac{v^2}{2} + U(y)\right)\right], \quad (2)$$

with the normalization constant k, and possess two maxima, corresponding to potential wells, separated by a saddle point of the potential. This structure does not depend on the noise intensity D: although the peaks in the PDF are smeared out, their position is invariant with respect to increase of noise intensity.

External random perturbations may result in the so-called noise-induced transitions whereby PDF of initially monostable system changes from single- to multi-peaked when noise intensity varies [18–21]. Such transitions occur both with multiplicative noise as in original Horthemke-Lefever scenario, and with additive noise (see, e.g. [22]). Although noise-induced transitions

are not true bifurcations [23], they underly qualitative changes of stochastic dynamics when noise strength is the control parameter. In this Letter we develop a generalized bistable oscillator with nonlinear dissipation and report on a multiple noise-induced transitions in this system. We first develop an electronic circuit model of the oscillator and demonstrate noise-induced transitions in analog experiment. Second, we use deterministic model and numerical simulations to explain mechanisms of noise-induced transitions.

Model and Methods – Fig. 1 shows a circuit diagram with two nonlinear elements N1 and N2 with the S- and N-type of the I-V characteristic, respectively: $i_{\text{N1}} = F(V)$, $V_{\text{N2}} = G(i)$. The circuit is similar to Nagumo's tunnel diode neuron model [24, 25], except it contains nonlinear resistor N2 in series with the inductor, L. The circuit also includes a source of broadband Gaussian noise current $i_{\text{noise}}(t)$, which will be assumed white in the following. The equations for the circuit in dimensionless form are (see Supplementary Material [26] for details on derivations):

$$\begin{cases} \varepsilon\dot{x} = -y - F(x) - \sqrt{2D}\, n(t), \\ \dot{y} = x - G(y), \end{cases} \quad (3)$$

where x is the dimensionless voltage, V, across the capacitor C, y is the dimensionless current i through the inductor L. The parameter ε sets separation of slow and
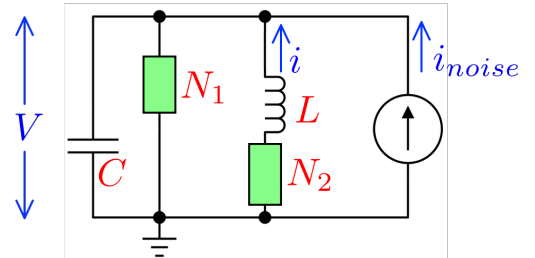

FIG. 1: (Color online) Circuit diagram of the model.

---

*corresponding author: semenov.v.v.ssu@gmail.com
†Electronic address: neimana@ohio.edu

fast variables of the system, $\varepsilon \sim C/L$. The first equation for the voltage contains an additive source of white Gaussian noise, $n(t)$, with the intensity D. Depending on the shape of the functions $F(x)$ and $G(y)$ the circuit demonstrates wide range of dynamics, including various types of bistability, self-sustained oscillations and excitability. It allows to observe a wide range of dynamical regimes: from the behavior like in oscillator (1) with a double-well potential to dynamics of an excitable oscillator or a bistable self-sustained oscillators. This letter is restricted to bistability of two stable equilibria with N-shape function $G(y) = -ay + by^3$ with positive coefficients a and b.

We start with a linear resistor N1, $F(x) = c_1 x$, with positive c_1. The circuit is described by,

$$\begin{cases} \dot{y} = v, \\ \varepsilon \dot{v} = -((3by^2 - a)\varepsilon + c_1)v - \\ (1 - c_1 a + c_1 by^2)y - \sqrt{2D}n(t). \end{cases} \quad (4)$$

The friction is nonlinear, but depends solely on the "coordinate" variable, y. For sufficiently small ε, $c_1 \gg \varepsilon(3by^2 - a)$ and dissipation becomes essentially linear. Then the system is closely akin to Kramers oscillator, Eq.(1), with *linear* friction. Our analog and numerical simulations showed no qualitative differences in dynamics of Kramers oscillator and the circuit (4) with linear resistor N_1, i.e. no noise-induced qualitative change in the stationary PDF.

Next, we consider the case of nonlinear resistor N1 with $F(x) = c_1 x - c_3 x^3 + c_5 x^5$ and with fixed positive coefficients $c_1 = 1, c_3 = 9, c_5 = 22$. A variety of the electronic elements and circuits have I-V characteristic like that. For example, N1 can be realized by the so-called lambda-diode circuit [27]. The circuit is described by the following "coordinate-velocity" equations, $y, v \equiv \dot{y}$, with $q(y, v) \equiv v - ay + by^3$,

$$\begin{cases} \dot{y} = v, \\ \varepsilon \dot{v} = -y - c_1 q + c_3 q^3 - c_5 q^5 + \\ \varepsilon v(a - 3by^2) - \sqrt{2D}n(t). \end{cases} \quad (5)$$

We note that unlike for the case of linear resistor N1, for the nonlinear N1 element, the system's dissipation depends on both coordinate and velocity, y and $\dot{y}$.

Experimental electronic setup was based on principles of analog modeling of stochastic systems [28, 29] and is described in details in the supplement [26]. State variables (y, v), time and parameters were transformed to dimensionless giving rise to Eqs.(5) [26].

Noise-induced transitions – Noise strength is true control parameter of the system, as Fig. 2 indicates. For weak noise, the circuit shows bistable dynamics with a typical hoping between two metastable states and two peaks in the PDF [Fig. 2(a1,b1)]. Increase of noise intensity leads to qualitative change in stochastic dynamics: hoping between two states disappears and so the PDF has a single global maximum, Fig. 2(a2,b2). Furthermore, larger noise results in yet another noise-induced transition whereby dynamics becomes bistable
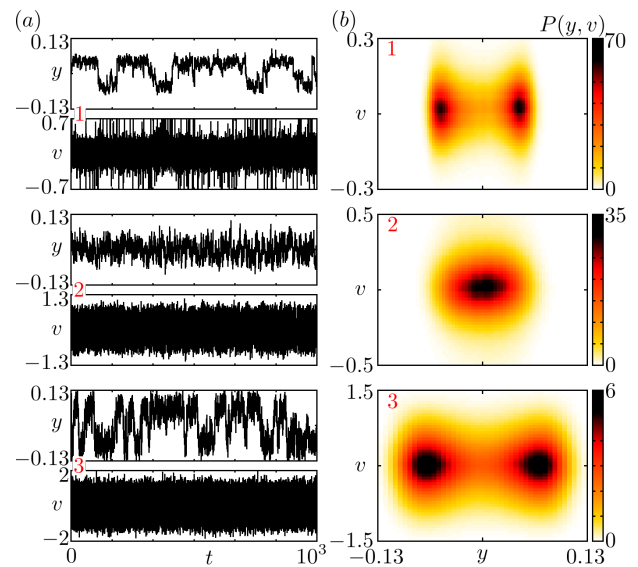

FIG. 2: (Color online) Noise-induced transitions in analog simulations. (a): Time traces of state variables for various values of noise intensity: $1 - D = 1.51 \times 10^{-4}$, $2 - D = 3.78 \times 10^{-4}$, $3 - D = 3.00 \times 10^{-3}$. (b): Stationary probability density functions (PDF) $P(y, v)$ corresponding to traces on (a). Other parameters are: $\varepsilon = 0.01, c_1 = 1, c_3 = 9, c_5 = 22, a = 1.2, b = 100$.

again with two-state hoping and double-peaked stationary PDF [Fig. 2(a3,b3)]. Noise-induced transitions are most apparent in a diagram of the marginal PDF of coordinate, $P(y) = \int_{-\infty}^{\infty} P(y, v)dv$ plotted vs noise intensity, D, in Fig. 3(d). This figure tracks positions of PDF's extrema vs D, showing two pitchfork bifurcations.

The described stochastic dynamics can be represented in terms of effective potential. The marginal PDF of the velocity variable, $P(v)$, is unimodal and the stationary PDF, $P(y, v)$, can be approximated by Eq.(2) with effective noise intensity and potential, $D_{\text{eff}} \to D$, $U_{\text{eff}}(y) \to U(y)$. The marginal velocity PDF, $P(v)$, is Gaussian in this approximation, and so the effective noise intensity is calculated as the velocity variance, $D_{\text{eff}} = \text{var}[v]$, i.e. from recorded time series. Fig. 3(a–c) shows that the marginal coordinate PDF, $P(y)$, can be nicely fitted by

$$P(y) = k_1 \exp\left[-\frac{1}{D_{\text{eff}}}U_{\text{eff}}(y)\right], \ U_{\text{eff}}(y) = -\alpha y^2 + \beta y^4, \quad (6)$$

where the parameters α, β, and k_1 are estimated from the least square fit of the experimentally measured marginal PDF, $P(y)$. The effective potential can be re-written in the form, $U_{\text{eff}}(y) = 4\beta(-\mu y^2/2 + y^4/4)$, with $\mu = \alpha/(2\beta)$. The shape of the effective potential, is determined by the effective bifurcation parameter, $\mu \equiv \mu(D)$. Thus, stochastic dynamics of the circuit can be described by the normal form of the pitchfork bifurcation [30], $\dot{z} = \mu z - z^3$: bistable for $\mu > 0$, monostable for $\mu < 0$ and critical at $\mu = 0$. Fig. 3(e) shows the dependence of the effective bifurcation parameter vs noise intensity, $\mu(D)$, and clearly
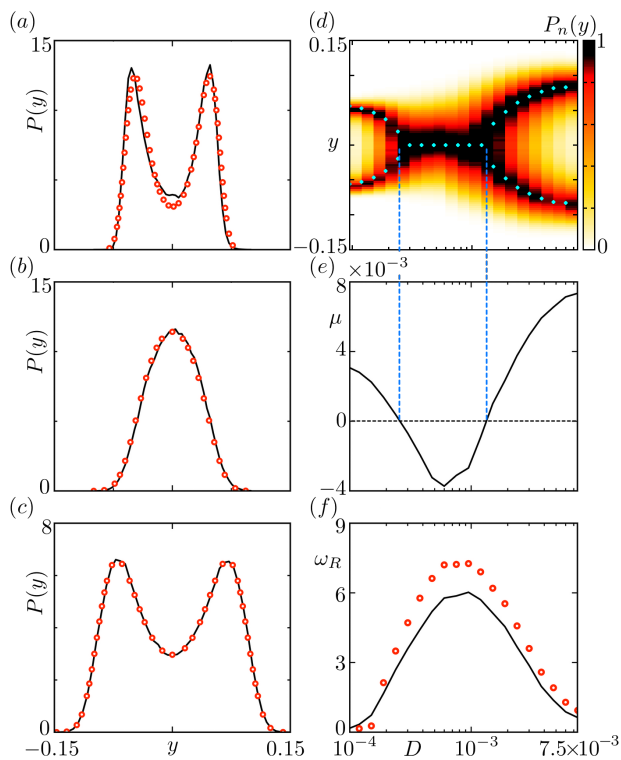
FIG. 3: (Color online) Noise-induced bifurcations in analog simulations. (a)–(c): Marginal PDF, $P(y)$ (lines) and its fit using the effective potential Eq.(6) (red circles). Noise intensity, effective potential parameters and effective noise intensity are: (a) $D = 1.51 \times 10^{-4}$, $\alpha = 14.35$, $\beta = 3193.5$, $D_{\text{eff}} = 1.15 \times 10^{-2}$; (b) $D = 3.78 \times 10^{-4}$, $\alpha = -9.71$, $\beta = 2532.4$, $D_{\text{eff}} = 4.07 \times 10^{-2}$; (c) $D = 3.00 \times 10^{-3}$, $\alpha = 76.12$, $\beta = 7707.1$, $D_{\text{eff}} = 2.35 \times 10^{-1}$. (d): Marginal PDF vs noise intensity. For each value of noise intensity, D, the PDF $P(y)$ was normalized to by its maximal value, i.e. $P_n(y) = P(y)/P_{\max}$. Blue dots track minima of the corresponding effective potential. (e): Effective bifurcation parameter $\mu(D)$. Vertical dashed lines indicate positions of two pitchfork bifurcations. (f): Rice frequency, ω_R, vs noise intensity. Solid line shows experimentally measured values; red circle correspond to approximation with Eq.(7) with the effective potential U_{eff}. Other parameters are the same as in the previous figure.

indicates two pitchfork bifurcations at $D = 2.6 \times 10^{-4}$ and $D = 1.34 \times 10^{-3}$ which match the bifurcation diagram, Fig. 3(d).

Stochastic bistable oscillators are characterized by two time scales: fast intrawell fluctuations and slower interwell switching. The mean frequency of bistable oscillator can be quantified by the Rice frequency [17, 31], which is the rate of zero-crossings by the oscillator's coordinate with positive velocity, $\omega_R = 2\pi \int_0^\infty v P(y=0, v) dv$. For

the Brownian oscillator (1) the Rice frequency reads [31],

$$\omega_R = \frac{\sqrt{2\pi D} \exp\left[-\frac{U(0)}{D}\right]}{\int_{-\infty}^{\infty} \exp\left[-\frac{U(y)}{D}\right] dy}. \tag{7}$$

For the bistable Kramers oscillator the Rice frequency increases with noise intensity, D [31], reflecting the increase of the Kramers rate of transitions between metastable states: the longer is the residence in metastable states, the smaller is the Karamers's rate and the Rice frequency. The dependence of the Rice frequency on noise intensity in our circuit is non-monotonous [Fig. 3(f)]: ω_R is low for weak and strong noise, where the system is bistable, and attains its maximal value for intermediate noise, corresponding to effective monostable dynamics with the deepest effective potential at the origin (minimal value of the bifurcation parameter, μ). Unlike for the Kramers oscillator (1), the velocity distribution, $P(v)$, for our bistable oscillator is non-Gaussian. Nevertheless the non-monotonous dependence $\omega_R(D)$ is well approximated by Eq.(7) with the effective potential and noise intensity, i.e. with the substitution $U_{\text{eff}} \to U$, $D_{\text{eff}} \to D$.

Mechanism of noise-induced transitions can be understood by studying the structure of the phase space of the deterministic circuit described by Eqs.(5). Fig. 4(a) shows two stable nodes, separated by the saddle at the origin, and nullclines of the system. The intrinsic feature of the system under study is an unusual structure of the nullcline $\dot{v} = 0$. Besides the conventional N-shape branch passing through equilibria [inset in Fig. 4(a)], the nullcline includes two symmetric separate closed-loop branches. Let us consider a loop at the upper left quadrant in Fig. 4(a). The upper side of the loop is attractive and lower one is repulsive. When a phase trajectory approaches the loop from above, it slows down and moves on the attractive side until it approaches the separatrix of the saddle, and then eventually falls onto vicinity of the saddle equilibrium at the origin. Repulsive side of the close-loop branch directs phase trajectories towards stable equilibrium. Symmetrical behavior occurs for the loop at the left lower quadrant. We note, that for the linear resistor N1 the nullcilne $\dot{v} = 0$ has a single N-shape branch only, i.e. no closed-loop segments.

Weak noise results in conventional stochastic hoping between two metastable states with the double-peaked PDF [Fig. 4(b)]. Note, that probability to cross closed-loop branches of the nullcline is rather low and so they have no effect on the position of the PDF's maxima. With the increase of noise intensity the PDF $P(y, v)$ smears vertically, i.e. with respect to velocity, v. Fig. 4(c) indicates, that phase trajectories frequently visit closed-loop branches [areas are marked by the green dashed line on Fig. 4(c)] which results in deflection towards the origin, as described for deterministic case on Fig. 4(a). This results in shifting of the PDF's maxima towards the origin. There is a critical noise intensity which corresponds to maximal influence of the closed-loop nullcline
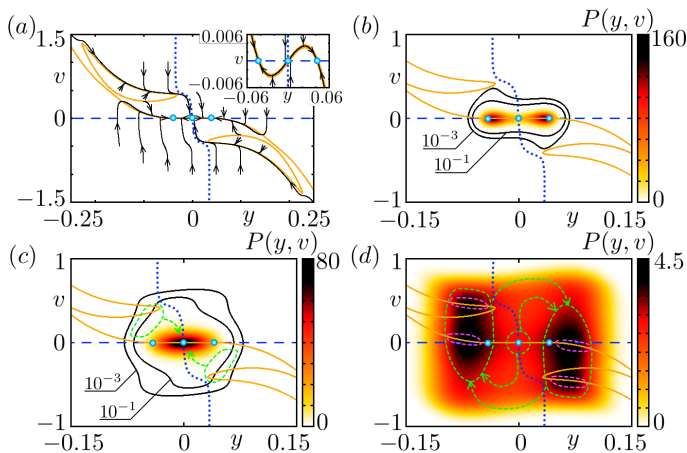
FIG. 4: (Color online) Mechanism of noise-induced pitchfork bifurcations. On all panels: equilibrium points are shown by blue circles; blue dashed line indicates the nullcline $\dot{y} = 0$; orange solid line shows the nullcline $\dot{v} = 0$; the separatrix of the saddle at the origin is shown by blue dotted line. (a): Deterministic dynamics of Eq.(5). Phase trajectories started from various initial conditions are shown by black arrowed lines. Inset shows expanded region near equilibria. Panels (b)–(d) also show contour maps of the stationary PDF, $P(y, v)$, obtained numerically. (b): $D = 2 \cdot 10^{-5}$; (c): $D = 6 \cdot 10^{-5}$; (d): $D = 2.4 \cdot 10^{-3}$. Other parameters are: $\varepsilon = 0.01, c_1 = 1, c_3 = 9, c_5 = 22, a = 1.2, b = 100$, i.e. the same as in analog experiments. See [26] for details on numerical procedure.

branches, resulting in the PDF with single peak at the origin. For larger values of noise intensity phase trajectories begin to pass through the repulsive sides of the closed-loop nullcline branches. They are then slow down on attractive branches of the nullcline [areas marked by violet dashed line on Fig. 4(d)] and then deflected towards the origin. However, because of larger noise, phase trajectories can now overcome the separatrix towards another stable equilibrium, rather than fall onto the origin. As a result, the origin is visited less frequently than symmetrical areas on the left and right of the separatrix. In this way the central peak of the PDF becomes divided into two and bistability is restored.

Conclusions – We have developed a generic model of the bistable oscillator with nonlinear dissipation. Using analog circuit experiment we showed that this system demonstrates multiple noise-induced transitions, registered as changes of extrema in the stationary PDF. Using the effective potential approach we showed that the observed noise-induced transitions are described by a normal form of pitchfork bifurcation. We provided a clear explanation of the mechanism of the effect based on partition of the phase space of the system by nullclines and manifolds of a saddle equilibrium.

[1] H. M. Gibbs, *Optical Bistability: Controlling Light with Light* (Academic Press, 1985).
[2] P. Hänggi, P. Talkner, and M. Borkovec, Rev. Mod. Phys. **62**, 251 (1990).
[3] H. Risken and T. Frank, *The Fokker-Planck Equation: Methods of solution and application.*, second edition ed., Springer Series in Synergetics (Springer-Verlag, Berlin, Heidelberg, 1996).
[4] H. Kramers, Physica **7**, 284 (1940).
[5] F. Schlögl, Zeitschrift für Physik **253**, 147 (1972).
[6] A. Goldbeter, *Biochemical Oscillations and Cellular Rhythms* (Cambridge University Press, Cambridge, 1997).
[7] G. Guidi, M.-F. Carlier, and A. Goldbeter, Biophysical Journal **74**, 1229 (1998).
[8] E. Ozbudak, M. Thattai, H. Lim, B. Shraiman, and A. van Oudenaarden, Nature **427**, 737 (2004).
[9] A. Shilnikov, R. L. Calabrese, and G. Cymbalyuk, Phys. Rev. E **71**, 056214 (2005).
[10] W. Smits, O.P.Kuipers, and J.-W. Veening, Nature Reviews Microbiology **4**, 259 (2006).
[11] R. Benzi, Nonlin. Processes Geophys. **17**, 431 (2010).
[12] R. M. May, Nature **269**, 471 (1977).
[13] V. Guttal and C. Jayaprakash, Ecological Modelling **201**, 420 (2007).
[14] R. Benzi, A. Sutera, and A. Vulpiani, Journal of Physics A: Mathematical and General **14**, 453 (1981).
[15] R. Benzi, G. Parisi, A. Sutera, and A. Vulpiani, Tellus **34**, 10 (1982).
[16] C. Nicolis, Tellus **34**, 1 (1982).
[17] J. Freund, L. Schimansky-Geier, and P. Hänggi, Chaos **13**, 225 (2003).
[18] W. Horsthemke and R. Lefever, *Noise-Induced Transitions* (Springer-Verlag, Berlin, Heidelberg, New York, 2006).
[19] A. B. Neiman, T. A. Yakusheva, and D. F. Russell, J. Neurophysiol. **98**, 2795 (2007).
[20] A. Zakharova, T. Vadivasova, V. Anishchenko, A. Koseska, and J. Kurths, Phys. Rev. E **81**, 011106 (2010).
[21] J. A. Kromer, R. D. Pinto, B. Lindner, and L. Schimansky-Geier, Eur. Phys. Lett. **108** (2014).
[22] L. Schimansky-Geier, A. Tolstopjatenko, and W. Ebeling, Physics Letters A **108**, 329 (1985).
[23] R. Toral *et al.*, AIP Conference Proceedings **1332**, 145 (2011).
[24] J. Nagumo, S. Arimoto, and S. Yoshizawa, Proceedings of the IRE **50**, 2061 (1962).
[25] E. M. Izhikevich and R. FitzHugh, Scholarpedia **1**, 1349 (2006).
[26] see supplemental material, where details of experimental

facility development and working are described .

[27] G. Kano, H. Iwasa, H. Tagaki, and I. Teramoto, Electronics **48**, 105 (1975).

[28] F. Moss and P. V. E. McClintock, eds., *Noise in Nonlinear Dynamical Systems: Vol. 3, Experiments and Simulations* (Cambridge University Press, Cambridge, 1989).

[29] D. Luchinsky, P. McClintock, and M. Dykman, Rep. Prog. Phys. **61**, 889 (1998).

[30] C. Meunier and A. Verga, Journal of statistical physics **50**, 345 (1988).

[31] L. Callenbach, P. Hänggi, S. J. Linz, J. A. Freund, and L. Schimansky-Geier, Phys. Rev. E **65**, 051110 (2002).

Supplemental material on Noise-induced transitions in a double-well oscillator with nonlinear dissipation

Proposed model and numerical methods – The electrical circuit which is an exemplary realization of the developed oscillator is presented in the paper [see Fig. 1 in the paper]. It is the circuit with parallel capacitance C and inductance L, including noise source $i_{noise}(t)$ and two nonlinear elements N1 and N2 with the I-V characteristics: $i_{N1} = F(V)$, $V_{N2} = G(i)$ (V is the voltage and i is the current). By using the Kirchhoff's current law the following differential equations for the voltage V across the capacitance C and the current i through the inductance L can be derived:

$$\begin{cases} C\dfrac{dV}{dt'} + i_{N1} + i + i_{noise}(t') = 0, \\ V = L\dfrac{di}{dt'} + V_{N2}. \end{cases} \quad (8)$$

In the dimensionless variables $x = V/V_0$ and $y = i/i_0$ with $V_0 = 1$ V, $i_0 = 1$ A and dimensionless time $t = [(V_0/(i_0L)]t'$, Eq.(8) can be re-written as,

$$\begin{cases} \varepsilon\dfrac{dx}{dt} = -y - F(x) - \xi(t), \\ \dfrac{dy}{dt} = x - G(y), \end{cases} \quad (9)$$

where $\varepsilon = (C/L)V_0^2/i_0$. The term $\xi(t)$ is assumed to be Gaussian white noise with zero mean and the intensity D: $\langle\xi(t)\rangle = 0$, $\langle\xi(t)\xi(t+\tau)\rangle = 2D\delta(\tau)$.

Numerical simulations were carried out by the integration of Eq. (9) by using the Heun method with time step $\Delta t = 0.0001$.

Experimental setup – The main part of the analog model is the operational amplifier integrator, whose output voltage is proportional to the input voltage integrated over time: $V_{out} = -\dfrac{1}{R_0C_0}\int_0^t V_{in}dt$ or $R_0C_0\dot{V}_{out} = -V_{in}$. Scheme of the experimental setup is shown in Fig. 5. It contains two integrators A1 and A10, whose output voltages are taken as the dynamical variables values x_* and y_* correspondingly. Then the signals x_* are y_* transformed in order to realize expressions corresponding to the right parts of the original system (Eq. (9)). The necessary signal transformations are carried out by using the analog multipliers AD633JN and the operational amplifiers TL072CP connected in the inverting and non-inverting amplifier configurations. Finally, obtained after transformation signals come to the input of the integrators as V_{in}. The experimental setup allows to analyze the instantaneous values of the variables x_*, y_* and the instantaneous value of the velocity which can be obtained by using x_* and y_* as being: $v_* = \dot{y}_* = x_* + ay_* - by_*^3$. Time realizations are taken at the corresponding outputs (are marked on the Fig. 5) and then processed in PC. An acquisition board (National Instruments NI-PCI 6133) is used for it. The

signals are acquired with a sampling frequency of 50 kHz. The Rice frequency and the probability density functions $P(y,v)$ and $P(y)$ are calculated by using realizations $y(t)$ and $v(t)$ with time length 150 seconds. The scheme in Fig. 5 is described by the following equations:

$$\begin{cases} R_xC_x\dfrac{dx_*}{dt_*} = -y_* - c_1x_* + c_3x_*^3 - \\ c_5x_*^5 - \xi(t_*), \\ R_yC_y\dot{y}_* = x_* + ay_* - by_*^3, \end{cases} \quad (10)$$

where $C_x = 30nF$, $C_y = 300nF$, $R_x = 1K\Omega$ is the resistance at the integrator A1 ($R_1 = R_2 = R_{13} = R_{20} = R_x = 1K\Omega$), $R_y = 10K\Omega$ is the resistance at the integrator A10 ($R_{14} = R_{19} = R_y = 10K\Omega$), parameter a is equal to the input value of the voltage V_a at the analog multiplier A14, $b = 10(1 + \dfrac{R17}{R18})$, $c_1 = 1$, $c_3 = 4(1 + \dfrac{R_5}{R_6})$, $c_5 = 0.4\dfrac{R7}{R8}$, $\varepsilon = \dfrac{R_xC_x}{R_yC_y}$. By the substitution $t = t_*/R_0C_0$, $x = x_*/V_0$, $y = y_*/V_0$, $v = v_*/V_0$, where $R_0C_0 = R_yC_y = 3$ milliseconds and $V_0 = 1$ Volt, Eq. (10) is reduced to Eq. (9) in the dimensionless variables x and y or to Eq. (5) in the paper in the dimensionless variables y and v.

System (10) was studied for the following parameters: $\varepsilon = 0.01$, $a = 1.2$, $b = 100$, $c_1 = 1$, $c_3 = 9$, $c_5 = 22$. There is also the noisy term in Eq. (10), generated by external noise generator. The generator G2-59 is used, it produces broadband Gaussian noise, whose spectral density is almost constant in the frequency range 0 – 100 kHz. In this frequency range noise can be approximated by white Gaussian. It's intensity, D', can be measured from the power spectral density of the noise generator signal. The noise intensity D' is related to dimensionless D used in the paper as $D = D'/(R_0C_0)$.
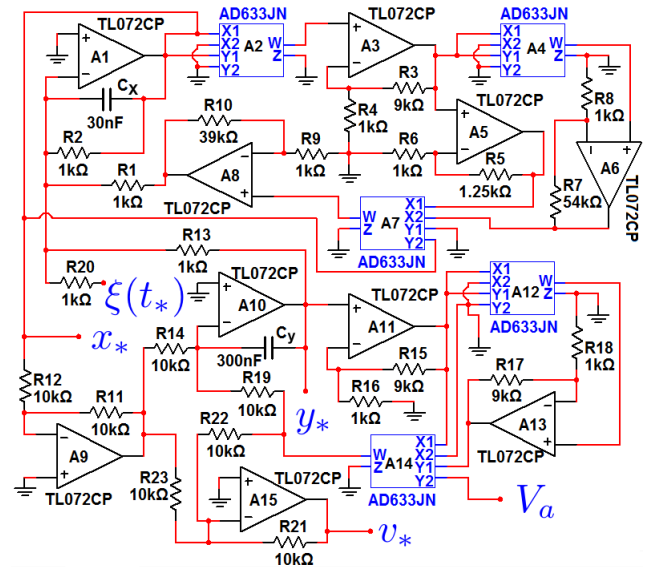

FIG. 5: Scheme of the experimental setup.